PHYSICAL REVIEW A VOLUME 19, NUMBER 1 JANUARY 1979

Statistical broadening and population loss in strongly excited three-level systems

J. R. Ackerhalt
Los Alamos Scientific Laboratory, Los Alamos, New Mexico 87545

J. H. Eberly*
Joint Institute for Laboratory Astrophysics, University of Colorado and National Bureau of Standards, Boulder, Colorado 80309

B. W. Shore
Lawrence Livermore Laboratory, Livermore, California 94550
(Received 27 December 1977)

We study the effects of statistical broadening and population loss on the dynamics of strongly excited three-level quantum systems. The results of both analytic and numerical treatments of the three-level Schrödinger equation are displayed. In order to allow for statistical broadening, solutions are required for arbitrary detuning of the two very intense monochromatic lasers. The most efficient statistically averaged population depletion occurs when the Rabi frequency of the second transition is greater than that of the first.

I. INTRODUCTION

The production of excited states of atoms and molecules has always been important for spectroscopic purposes. It is useful to know how to produce highly selected excited states in quantities as large as possible.

One method for doing this relies on the ability of nearly monochromatic lasers to stimulate upward transitions in atoms or molecules. Once the atom or molecule reaches an appropriate excited state, it is studied in some way. This process usually involves an irreversible interaction of some kind, perhaps deexcitation, ionization, or dissociation, with consequent removal from the studied sample. A general photoexcitation-plus-reaction sequence can be sketched as in Fig. 1.

It appears, on simple heuristic grounds, that the more powerful and monochromatic the lasers are, and the closer they are tuned to resonance with the favored atom or molecule, the greater will be the extent of the desired reaction. Most experimental studies to data of multilevel and multiphoton applications have been based on this simple notion. Such arguments are valid only if the absorption processes are describable by rate constants; that is, if the population of each successively higher level of the atom or molecule grows smoothly at a rate proportional to the population of the level below it. When such a picture is accurate we can speak of being in the "rate regime" of absorptive interaction.

However, when the stimulated transition rate is too high, this rate-regime picture is not accurate and the rate constant is not a reliable gauge of the transition process. Instead of smooth population flow from one level to the next, one then finds population oscillations breaking out. The extreme limit of this process is just the multilevel analog of the long-studied Rabi oscillations of two-level systems.[1] We will say that we are in the "Rabi regime" when such population oscillations are the dominant feature of an absorptive interaction. If the number of near-resonant levels involved is greater than two, the theory of the Rabi regime is much more complicated than rate-regime theory, and it is necessary to employ numerical techniques almost exclusively. Nevertheless, recent

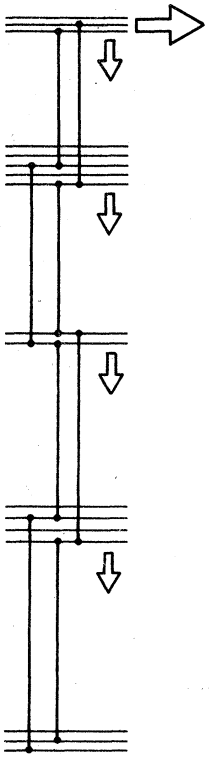

FIG. 1. Schematic representation of photoexcitation, relaxation, and reaction of an atom or molecule. The vertical lines represent laser-stimulated emission and absorption transitions. The vertical arrows represent laser-independent relaxation; and the horizontal arrow represents relaxation via population loss out of the system. Horizontal lines represent different states associated with each energy level.

work has clarified the general characteristics of population flow in multilevel systems in the Rabi regime[2] and a few analytic results are available in special cases[3] to describe population flow in multilevel systems when the laser power is so high that population oscillations are dominant.

It is helpful to associate each of these two regimes with a simplified model of the radiative excitation of the "real" atom or molecule depicted in Fig. 1. The model associated with the rate regime is one in which each level has a well-defined width and in which population flows only upward, under the influence of fields that are not too strong. On the other hand, the extreme Rabi-regime atomic model is characterized by zero linewidths, a zero reaction rate at the top, and a significant population flow in both directions. These two models are shown in Figs. 2(a) and 2(b).

Although the Rabi-regime theory is much more fundamental in many respects than the rate-regime theory, it is inferior in an important way. Because the Rabi-regime theory concentrates just on the oscillations of the level populations, that is, on the coherent and phase-preserving features of the interaction between laser and atom or molecule, it must reflect very poorly the physics of the final reaction stage in any of the applications sketched above. This is because an ionization,

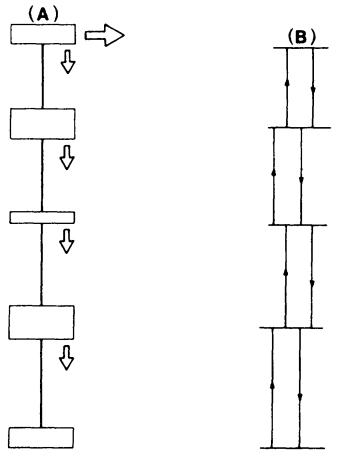

FIG. 2. (a) Schematic representation of an atom or molecule undergoing photoexcitation and relaxation in the rate regime. The existence of separate states within a level is not recognized and the levels are simply assigned a featureless width s determined by their relaxation rates. (b) Schematic representation of an atom or molecule undergoing photoexcitation in the Rabi regime. The levels are taken to be sharp, and population-loss relaxation is ignored. The vertical lines are drawn with arrows to indicate that strong laser-induced population cycling, downward as well as upward, is the primary feature of the dynamical behavior.

dissociation, reaction, or collection event is almost certainly irreversible, and therefore completely phase destructive and incoherent. Since the ultimate reaction process should be made as efficient as possible, it is highly unrealistic to ignore completely its incoherent effect on the system's population dynamics. Unfortunately, the problem of incorporating the reaction into the theory cannot be solved simply by the expedient of assuming that it is so large that it dominates the dynamics of the final level. This is so for two suitably. In the first place, it has been shown[4] that if the power levels of the lasers involved are suitable arranged, a large degree of incoherence in the last level can be transferred to all of the levels, destroying the coherence of the entire system and placing its absorptive behavior squarely in the rate regime. In the second place, the limit of very large reaction rate must be avoided for practical reasons: contrary to what might be expected at first thought, a large irreversible reaction rate acting on the last level is actually counterproductive, leading to a decrease in collected reactant.[5]

The difficulties faced in modeling phase-destroying collection from the highest level together with phase-coherent oscillations in lower levels can be overcome numerically. Both of the extreme models shown in Fig. 2 and a number of intermediate cases have been discussed recently in the three-level case.[6]

However an important feature of the "real" atom or molecule undergoing both excitation interactions and a collection reaction, as shown in Fig. 1, has not yet been investigated in multilevel and multiphoton absorption. Figure 1 reminds us that in any absorber there may be several or many paths from the ground level to the reaction-collection level. We have indicated these alternative paths by sketching a few sublevels associated with each principle level. These alternative paths can be distinguished from each other, for example by dipole moment, by angular momentum quantum number, by transition frequency, or by combinations of these. In a molecule, the alternative paths could arise from the rotational sublevels associated with a vibrational level. In an atom a variety of alternative paths could arise from the existence of hyperfine or Zeeman splittings, or from the range of possible transition frequencies implied by the Doppler widths of the levels. Whatever their origin, these sublevels and their associated alternative upward paths create enormous complications for the theory.[7]

In this paper, we take a step toward the realistic case by incorporating both a manifold of sublevels associated with each principle level, as

well as a finite collection rate from the highest level. We are not able to deal with the general N-level system, and are restricted to numerical methods at most stages of analysis, but we can obtain some analytic as well as numerical solutions for a variety of cases when $N=3$. As our main interest will be in the qualitative effect of the sublevels, our choice of a particular value, namely 3, for N does not seem unduly restrictive.

The approach we will use to incorporate sublevels, without becoming swamped in the details of the magnetic quantum numbers and dipole moments of each sublevel's transitions, is motivated as follows. We assume as in Fig. 1 that all of the sublevel sequences participate independently in the absorption process, and that the dipole moments are near enough to being the same that we can call them equal. However, the resonant character of the interaction of the laser with the atom or molecule is central to successful and efficient absorption. For this reason, we retain a specific frequency label for each sublevel. Most of the sublevels will be out of resonance with the laser and only a very narrow band will be close to resonance, for any given laser tuning. Furthermore, to avoid the arbitrariness of an assumption about exactly how many sublevels are attached to a given principle level, we assume that there is a continuous distribution of sublevels, characterized by a sublevel bandwidth function, for each principle level. One may call our approach a statistical (or inhomogeneous) broadening approach to the sublevel problem. The absorbing system implied by such a statistical broadening assumption might be sketched as shown in Fig. 3. The line shape used below is Gaussian.

Our model gives an accurate quantitative picture of the effect of Doppler broadening on multistage absorption in both atomic and molecular gases, and we make use of this feature to investigate the possible advantages of Doppler-free excitation and reaction as well. We expect that the results obtained from our oversimplified version of the alternative absorption paths of real atoms and molecules will also be at least qualitatively relevant to the multilevel and multiphoton absorption problem in a variety of other cases including the hyperfine-broadened case for atoms, and the rotationally broadened case for molecules.

A preview of the paper's contents can be given briefly. We study the excitation-plus-reaction dynamics of three-level systems stimulated by two coherent light sources. We consider a variety of relative intensities of the two sources, allowing both copropagating and counterpropagating light beams. We allow population loss from the third level such as might be due to chemical reaction,

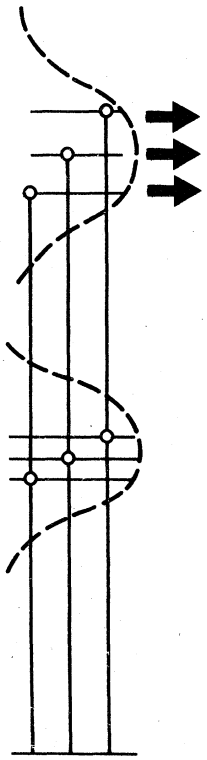

FIG. 3. Schematic representation of a three-level atom or molecule undergoing statistically broadened photoexcitation. The energy levels consist of identifiable states spread over a finite range of energies, and the states of the upper level can undergo relaxation due to population loss. The dynamics may be characterized by stimulated rate processes as in the rate regime, or by coherent population cycling as in the Rabi regime.

or relaxation to a fourth level. Our objective is to find effective techniques for reacting as large a portion of the inhomogeneous distribution as possible.

In the following sections, we display examples of both analytical and numerical solutions of the three-level Schrödinger equation. For simplicity, we refer to the reaction mechanism as ionization and to the statistical distribution of detuning as a Doppler average. We show both the on-resonance level populations $P_n(t;\Delta=0)$ and ionized population $P_{\text{ion}}(t;\Delta=0)$ as well as the ensemble averages $\overline{P}_n(t)$ and $\overline{P}_{\text{ion}}(t)$ (obtained by numerical quadrature of the distribution integral). By means of such examples, we demonstrate the dependence of solutions upon the basic model parameters, the two Rabi frequencies Ω_1 and Ω_2, the reaction rate R, and the width of the statistical distribution of detinings, denoted $1/T^*$.

We exhibit the Schrödinger dynamics as a function of the laser powers with all other parameters fixed. The statistical width $1/T^*$ is scaled to unity. The reaction rate R in level 3 provides a nonstatistical (homogeneous) linewidth, chosen smaller than $1/T^*$:

$$R=\tfrac{1}{6}(1/T^*).$$

For example, $R=10^9$ sec^{-1} corresponds to a Doppler half width of about 2 GHz. We will follow the

evolution of the level populations for ten "reaction times" $10/R$. The interesting region to study the growth of reactant versus laser power occurs where the Rabi frequencies are close in value to the statistical width:

$$\tfrac{1}{4}(1/T^*)\leq(\Omega_1,\Omega_2)\leq 4(1/T^*).$$

The behavior for smaller values of Ω is expected to be dominated by the nonstatistical reaction rate R, and for larger values to consist primarily of weakly smoothed pure Rabi oscillations.

II. THREE-LEVEL ROTATING-WAVE-APPROXIMATION MODEL

Our three-level systems have energy levels E_1, E_2, and E_3, excited by two monochromatic lasers whose frequencies ω_1 and ω_2 are close to the Bohr transition frequencies $\bar{\omega}_1=(E_2-E_1)/\hbar$ and $\bar{\omega}_2=(E_3-E_2)/\hbar$. We call this system an atom, although our results apply equally well to a molecular system. Figure 3 symbolizes the excitation sequence of one such atom. We express the three-level state vector $\psi(t)$ as a three-component superposition of basis states ϕ_n

$$\psi(t)=\sum_{n=1}^{3}C_n(t)\phi_n\exp(-i\alpha_n)$$
$$=C_1(t)\phi_1+C_2(t)\phi_2e^{-i\omega_1t}+C_3(t)\phi_3e^{-i\omega_2t}. \qquad (2.1)$$

The phases α_n implicit in any such expansion are, of course, arbitrary. We express them in terms of the light frequencies, thereby employing the rotating-wave picture; in the Schrödinger picture the phases are identically zero whereas in the Dirac (or interaction) picture the phases are the Bohr frequencies.

Because the three levels are intended to represent the real atom, with infinitely many levels, in its interaction with an external "reaction" mechanism as well as with two lasers, the matrix elements of the Hamiltonian within the three-element subspace are generally complex and non-Hermitian. Diagonal elements have the form

$$H_{nn}=E_n-\tfrac{1}{2}i\Gamma_n, \qquad (2.2)$$

where $\Gamma_n/\hbar$ is the rate at which probability is irreversibly lost into the reaction channel. We shall assume that such loss occurs only from level 3 at a rate R. This loss may originate in many ways, for example, via collisions, tunneling in static fields, photoionization, autoionization, etc. We assume that the energies E_n and the Bohr frequencies $\bar{\omega}_1$ and $\bar{\omega}_2$ are time independent (because we assume cw or long-pulse lasers), and that they incorporate all laser-dependent shifts.

We assume that the lasers are sufficiently intense that stimulated emission dominates spontaneous emission. Thus we express the laser fields as prescribed classical harmonic functions of time. The nonzero matrix elements of the atom-field interaction can then be written

$$H_{12}=H_{21}=-\hbar\Omega_1^{(1)}\cos(\omega_1t)-\hbar\Omega_1^{(2)}\cos(\omega_2t),$$
$$H_{23}=H_{32}=-\hbar\Omega_2^{(2)}\cos(\omega_2t)-\hbar\Omega_2^{(1)}\cos(\omega_1t). \qquad (2.3)$$

Here $\Omega_n^{(m)}$ is the interaction-energy frequency, or Rabi frequency,[1] for the nth transition, associated with the mth laser.

Upon substituting expansion (2.1) into the Schrödinger equation

$$i\hbar\frac{d}{dt}\psi(t)=H(t)\psi(t) \qquad (2.4)$$

and using formulas (2.2) and (2.3), we obtain the set of coupled equations

$$i\frac{d}{dt}C_n(t)=\sum_m W_{mn}(t)C_n(t). \qquad (2.5)$$

The time dependence of W occurs only in off-diagonal elements. For example, one easily finds

$$W_{12}(t)=\tfrac{1}{2}\Omega_1^{(1)}\{1+\exp[i(\omega_1+\omega_2)t]\}$$
$$+\tfrac{1}{2}\Omega_1^{(2)}\{\exp[i(\omega_1-\omega_2)t]+\exp[i(\omega_1+\omega_2)t]\}. \qquad (2.6)$$

The atom responds to these forces on a time scale set by the Rabi frequencies. We assume that this response time is much slower than the occurring sum and difference frequencies,

$$|\Omega_1^{(1)}|\approx|\Omega_1^{(2)}|\ll|\omega_1-\omega_2|\lesssim\omega_1,\ \omega_2,\ \omega_1+\omega_2, \qquad (2.7)$$

so that we can replace such oscillating terms by their null time average.

One physical distinction between photoexcitation of atoms on one hand, and molecules on the other, should be mentioned. If the molecular levels are nearly harmonic, so that $\bar{\omega}_1\approx\bar{\omega}_2$, then it is very hard to satisfy $|\omega_1-\omega_2|\gg|\Omega|$ within the near-resonance context in which $\omega_1\approx\bar{\omega}_1$ and $\omega_2\approx\bar{\omega}_2$. But then the second laser is unnecessary, and only one term in Eqs. (2.3) is sufficient. In atoms $\bar{\omega}_1\approx\bar{\omega}_2$ occurs very rarely.

Upon dropping the rapidly oscillating terms we obtain the usual rotating-wave approximation[1] (RWA) for either atoms or molecules:

$$W_{12}\cong\tfrac{1}{2}\Omega_1^{(1)}\equiv\tfrac{1}{2}\Omega_1,\quad W_{23}\cong\tfrac{1}{2}\Omega_2^{(2)}\equiv\tfrac{1}{2}\Omega_2, \qquad (2.8)$$

yielding the time-independent RWA matrix

$$W=\begin{pmatrix}0 & -\frac{1}{2}\Omega_1 & 0\\ -\frac{1}{2}\Omega_1 & \Delta_1 & -\frac{1}{2}\Omega_2\\ 0 & -\frac{1}{2}\Omega_2 & \Delta_1+\Delta_2-i\frac{1}{2}R\end{pmatrix}, \qquad (2.9)$$

where Δ_n is the detuning of the nth laser frequency away from the corresponding Bohr frequency:

$$\hbar\Delta_1=(E_2-E_1)-\hbar\omega_1, \tag{2.10a}$$

$$\hbar\Delta_2=(E_3-E_2)-\hbar\omega_2. \tag{2.10b}$$

III. STATISTICAL AVERAGES

The statistical ensemble comprises a distribution of atomic or molecular detunings. It is the nature of Doppler broadening that if the atoms or molecules at rest are resonant at each successive upward transition, then the atoms or molecules in motion find each successive upward transition further off resonance. If the transition frequencies are nearly equal, then a two-photon transition will be twice as far above or below resonance as will the one-photon transition. For copropagating laser beams this is true. Both transitions experience Doppler shifts in the same direction. The one-photon detunings are

$$\Delta_1\cong\omega_1 v/c\equiv\Delta, \quad \Delta_2\cong\omega_2 v/c\simeq\Delta, \tag{3.1}$$

where v is the component of velocity along the lasers' common axis. The two-photon detuning is the sum of these

$$\Delta_1+\Delta_2\cong 2\Delta. \tag{3.2}$$

Note that Eq. (3.1), which implies that $|\Delta_2-\Delta_1|$ is negligibly small, is not in conflict with the requirement in Eq. (2.7) that $|\omega_2-\omega_1|$ be large, because v/c is so small.

To indicate the implicit dependence of the probability amplitudes upon detuning we employ the notation $C_n(t;\Delta)$. Then the probability of observing the atom having detuning Δ in level n at time t is

$$P_n(t;\Delta)=|C_n(t;\Delta)|^2 \tag{3.3}$$

and the probability of finding the atom ionized is

$$P_{\text{ion}}(t;\Delta)=1-\sum_{n=1}^{3}P_n(t;\Delta). \tag{3.4}$$

The corresponding statistical averages over detuning are

$$\overline{P}_n(t)=\int_{-\infty}^{\infty}d\Delta\, g(\Delta)P_n(t;\Delta) \tag{3.5}$$

and

$$\overline{P}_{\text{ion}}(t)=1-\sum_{n=1}^{3}\overline{P}_n(t). \tag{3.6}$$

We shall take the statistical weighting function $g(\Delta)$ to be a Gaussian distribution,

$$g(\Delta)=(T^*/\pi)\exp[-(1/\pi)(\Delta T^*)^2] \tag{3.7}$$

as is appropriate to Doppler broadening. We measure the width of the distribution by T^*, the statistical (inhomogeneous) relaxation time of the system. It is related to the laser wave vector k and mean atomic velocity u by

$$(ku)^2=\pi/(T^*)^2, \tag{3.8}$$

and to the half width at half maximum $\Delta_{1/2}$ by

$$\Delta_{1/2}=(\pi\ln 2)^{1/2}(1/T^*)\cong 1.5/T^*. \tag{3.9}$$

The Schrödinger equation (2.5) with the RWA Hamiltonian (2.9) can be solved exactly by finding the roots to a cubic equation. The solutions are very complicated in the general case, even for fixed values of Δ_1 and Δ_2. However, our main interest is in atomic or molecular systems with a range of transition frequencies. The integrations over Δ_1 and Δ_2 must be carried out numerically in any event, so we simply solve the time-dependent Schrödinger equation numerically as well, and display the results graphically. In Secs. V and VI we will find it useful to contrast some of these numerical results with approximate analytic solutions, and with recent experimental observations.

IV. EQUAL RABI FREQUENCIES

To establish the basic features of the statistically broadened excitation and reaction process that are common to all cases we first consider the special case in which the two Rabi frequencies are equal: $\Omega_1=\Omega_2$. Figures 4(a)–4(c), show the behavior of each of the resonant populations $P_n(t;0)$ together with their sum, and the ionization probability $P_{\text{ion}}(t;0)$. We observe the familiar Rabi population oscillations. These grow progressively more rapid with increasing interaction strength. The ionization probability grows until saturated, modulated by the Rabi oscillations.

In Figs. 5(a)–5(c) we exhibit the statistical averages $\overline{P}_n(t)$ and $\overline{P}_{\text{ion}}(t)$. This shows the effect of averaging over an ensemble of different transition frequencies the cases whose resonance ($\Delta=0$) populations appear in Figs. 4(a)–4(c).

The curves of Figs. 4(a) and 5(a) pertain to Rabi frequency $\frac{1}{4}$ and ionization rate $\frac{1}{8}$. Figures 4(b), 5(b), 4(c), and 5(c) show the same quantities: resonant populations, Doppler averaged populations, and ionization profile, for Rabi frequencies 1 and 4 (that is, for power levels 16 and 256 times greater), respectively.

In the statistical averages, we have the combination of the resonance transition and the complete ensemble of nonresonant transitions, whose excitation and ionization is less complete and whose populations oscillate more rapidly. Their oscillation frequency is the rms value of their resonant Rabi frequency and their detuning. Because of the Gaussian weighting function $g(\Delta)$,

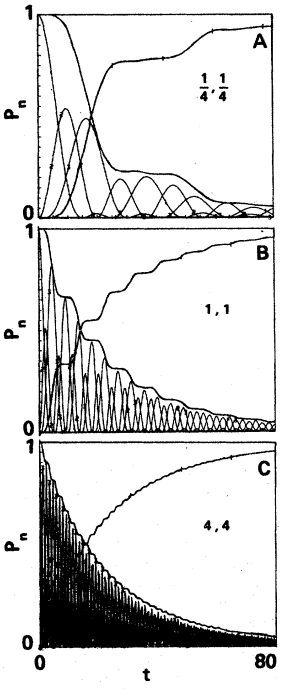

FIG. 4. Level probabilities $P_n(t;0)$ for three-level system undergoing on-resonant excitation by two lasers. Solid curves labeled 1, 2, 3 show populations of individual levels vs time, dotted curve labeled I is reacted (ionized) fraction, unlabeled dotted line is the sum of bound-state probabilities. Frame (a): Rabi frequencies $\Omega_1=\Omega_2=\frac{1}{4}$; frame (b): $\Omega_1=\Omega_2=1$; frame (c): $\Omega_1=\Omega_2=4$. All cases have reaction (population-loss) rate $R=\frac{1}{8}$.

the major contribution to the statistical average comes from transitions that are, at most, a few times $1/T^*$ away from resonance. When Ω is much smaller than $1/T^*$, as it is in Figs. 4(a) and 5(a) (where $\Omega/T^*=\frac{1}{4}$), almost the entire contribution to $\bar{P}_n(t)$ comes from atoms whose behavior differs little from the resonance case $P_n(t;0)$. When the Rabi frequencies are much greater than the relaxation rate $1/T^*$, as they are in Figs. 4(c) and 5(c) (where $\Omega T^*=4$) the contributions to $\bar{P}_n(t)$ from off-resonance atoms are nearly equally as effective as the resonant contributions. As a result, the statistical average is much more effectively excited and ionized when $\Omega \gg 1/T^*$.

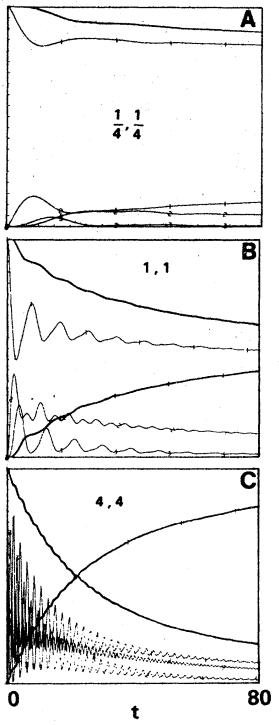

FIG. 5. Level probabilities $\bar{P}_n(t)$ for the three cases of Fig. 4, but populations are averaged over a statistical distribution of detunings as in Eq. (3.5). The distribution width $1/T^*$ is taken equal to 1.

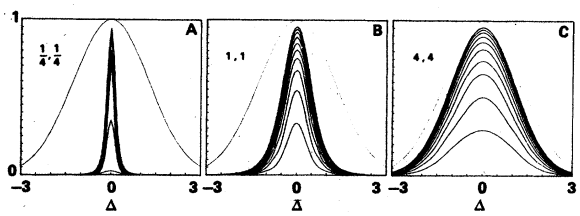

FIG. 6. Dotted curve shows distribution of relative atomic populations $P_n(t;\Delta)$ as a function of detuning; solid curves show, at a succession of ten equidistant times $\Delta t=1/R$ out to $t=80$, the ionized fraction of this statistical distribution as a function of detuning. The three frames correspond to the parameter choices of Fig. 4: Frame (a): $\Omega_1=\Omega_2=\frac{1}{4}$; frame (b): $\Omega_1=\Omega_2=1$; frame (c): $\Omega_1=\Omega_2=4$.

Note that, although the averaged ionization curve approaches the resonance-case ionization curve as the Rabi frequencies become much larger than the relaxation rate, nevertheless the averaged individual level populations do not in general approach the corresponding resonance-case populations. Only during a time interval smaller than T^* are the population curves $P_n(t;0)$ and $\bar{P}_n(t)$ closely similar. At later times, the population average $\bar{P}_n(t)$ oscillates at the frequency of $P_n(t;0)$ but with reduced amplitude. As we should expect, we see that increasing the laser intensity (by increasing the Rabi frequency) leads to an increase at each instant in the distribution of detunings which can ionize. This is "power broadening" of the ionization profile.

In Figs. 6(a)–6(c) we show the contributions of various detunings Δ to the total ionization probability, at a succession of times $t=1/R$, $2/R, \ldots, 10/R$, where R is the ionization rate from level 3. We have plotted here with the full lines the product

$$P_{\text{ion}}(t;\Delta)g(\Delta)/g(0)$$

representing relative ionization probability, and with the dotted lines the envelope $g(\Delta)/g(0)$ representing the upper limit to this ionization. The three cases shown correspond to the three cases of Figs. 4 and 5, namely, $\Omega_1=\Omega_2=\frac{1}{4}, 1, 4$.

V. UNEQUAL RABI FREQUENCIES

Section IV showed the effect of averaging the three-level population dynamics over an ensemble of different transition frequencies when the two Rabi frequencies were equal. Here we consider a more interesting series of cases in which the first Rabi frequency gets progressively larger, viz., the sequence

$$(\Omega_1, \Omega)=(\tfrac{1}{2},\tfrac{1}{2}),\ (1,\tfrac{1}{2}),\ (2,\tfrac{1}{2}),$$

and then we consider the opposite situation, a sequence in which the second Rabi frequency is larger:

$$(\Omega_1, \Omega_2)=(\tfrac{1}{2},\tfrac{1}{2}),\ (\tfrac{1}{2},1),\ (\tfrac{1}{2},2).$$

As we show, the two situations lead to results that are different both qualitatively and quantitatively.

A. Numerical experiments

First we study the on-resonance situation. Figure 7 shows the time-dependent populations for the on-resonance member of the statistical ensemble. In this figure, the top frame has equal Rabi frequencies; down the left-hand side the second Rabi frequency increases.

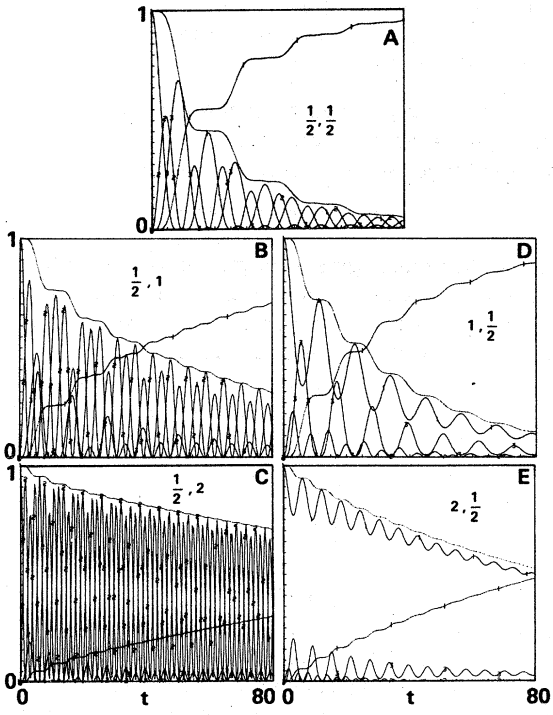

FIG. 7. Level populations $P_n(t;0)$ for resonantly tuned excitation. Left-hand sequence of frames (a)–(c) have increasing values of $\Omega_1=\frac{1}{2},1,2$; right-hand frames a, d, e have increasing values of $\Omega_2=\frac{1}{2},1,2$. Frame (a): $\Omega_1=\frac{1}{2}$, $\Omega_2=\frac{1}{2}$; frame (b): $\Omega_1=1$, $\Omega_2=\frac{1}{2}$; frame (c): $\Omega_1=2$, $\Omega_1=\frac{1}{2}$; frame (d): $\Omega_1=\frac{1}{2}$, $\Omega_2=1$; frame (e): $\Omega_1=\frac{1}{2}$, $\Omega_2=2$. All cases have $R=\frac{1}{8}$.

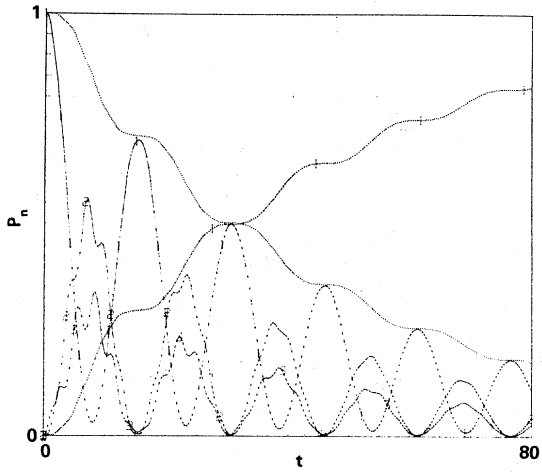

FIG. 8. Populations $P_n(t;\Delta)$ for case $\Omega_1=\frac{1}{2}$, $\Omega_2=2$ when first laser is detuned by amount approximately equal to the dynamic Stark shift $\Delta=0.640$.

We see that ionization proceeds more effectively when the stronger laser drives the second transition. We also see that, when the first laser is stronger, populations in levels 1 and 2 oscillate with increasing rapidity and level 3 plays a decreasing role, as the Rabi frequency increases. In effect our system reduces to a two-level atom weakly coupled to a third level. This behavior has been studied[8] in many cases not involving statistical averaging, and has been observed recently in ionization.

A second striking difference appears in the degree of population modulation which occurs. We see this quite clearly in the two bottom frames. The incomplete modulation in Fig. 7(e) indicates that, although we are considering the resonant transition, $\Delta=\bar{\omega}_1-\omega_1=0$, the atom is not really on resonance. The presence of intense laser 2 has split the position of resonance in transition 1 by the dynamic Stark shift.[9] If we detune the first laser by 0.640 we obtain, in place of Fig. 7(e), Fig. 8. Here the modulation is nearly complete between level 1 and a combination of levels 2 and 3.

Now we proceed to a discussion of the same sequences of cases, but focusing this time on a statistical average of all atoms. Figure 9 shows the averaged populations. From Figs. 9(b) and 9(c) wherein Ω_2 is fixed, we observe that the ionization versus time is very nearly independent of the intensity of laser 1. On the other hand, Figs. 9(d) and 9(e) show that the total ionization does increase with increasing Ω_2. Note that the statistically averaged population oscillations in Fig. 9(e) are approximately one-half as frequent as the on-reso-

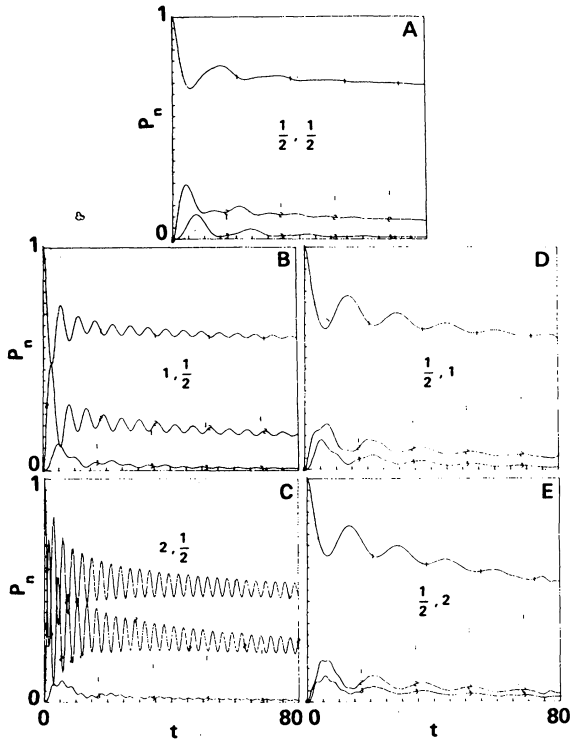

FIG. 9. Population averages $\bar{P}_n(t)$ over statistical distribution with $T^*=1$. Parameters are the same as Fig. 6.

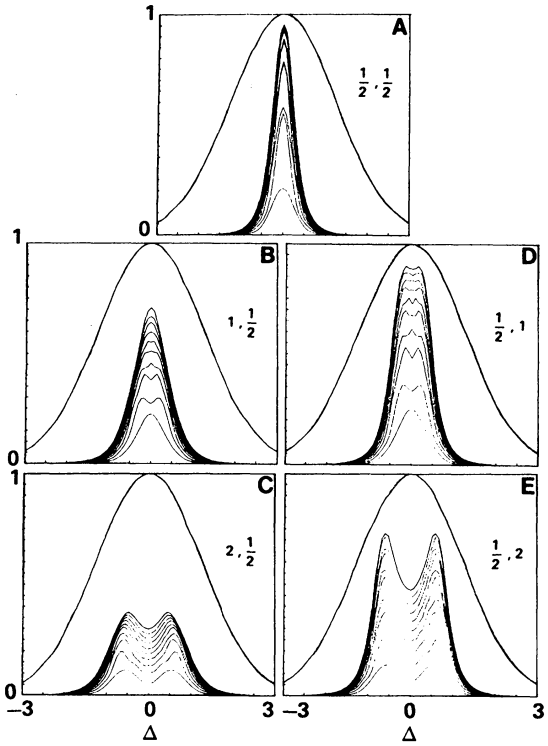

FIG. 10. Relative ionization probability $P_{\text{ion}}(t;\Delta)$ at successive times, as a function of detuning. Parameters are the same as Fig. 6.

nance oscillations in Fig. 7(e).

Figure 10, like Fig. 6 shows the relative ionization probability at successive times for the preceding cases.

As either laser power is increased, we see, as expected, a power broadening of the ion output. The single-peak structure which exists for equal Rabi frequencies becomes a doublet if either Rabi frequency is much larger than the other. This doublet structure can be interpreted as the dynamic Stark effect.[9] Since in Figs. 10(c) and 10(e) one Rabi frequency is much greater than the other, in each case we can consider the three-level atom as a "dressed" two-level atom weakly coupled to a third level. The two peaks in the ionization rate correspond to laser-atom detunings which are located at resonances of the "dressed" two-level atom. Since the structure is independent of which Rabi frequency is larger, the interpretation must also be independent of which Rabi frequency is larger.

While the structure is independent of which Rabi frequency is larger, the overall ionization is not. A greater number of atoms are ionized if $\Omega_2 > \Omega_1$. This means that more ions are produced if the "dressed" atom is associated with transition 2. A larger Rabi frequency for transition 2 means a greater power broadening which more effectively overlaps the very broad Doppler width of level 3 thereby increasing the overall ionization.

B. Theoretical analysis

It is possible to give a nonperturbative analysis of a few of the features of Figs. 7–10, in particular the pronounced doublet structure in Figs. 10(c) and 10(e) and the increased ionization when $\Omega_2 > \Omega_1$. It is helpful to use the idea of "dressed" states[10] in order to facilitate such an analysis. Consider a two-level system with the RWA Hamiltonian shown below

$$W_2 = \begin{pmatrix} a & -\frac{1}{2}\Omega \\ -\frac{1}{2}\Omega & b \end{pmatrix}. \tag{5.1}$$

If the coupling strength Ω between the two states is very strong, so that $\Omega \gg a, b$, it is as if the two levels are, in effect, degenerate. In such a case it is appropriate to remove the quasidegeneracy before proceeding with a treatment of the dynamics. Note that when R is relatively small and Ω_1 and Ω_2 are comparable with or larger than $1/T^*$, then the upper-left and lower-right corners of W given in (2.9) are 2×2 matrices with this same kind of quasidegeneracy.

The unitary transformation that lifts the quasi-

degeneracy (i.e., "dresses" the two states) is

$$U=\begin{pmatrix}\cos\phi & -\sin\phi\\ \sin\phi & \cos\phi\end{pmatrix}, \tag{5.2}$$

where

$$\sin 2\phi=-\Omega/[(b-a)^2+\Omega^2]^{1/2}, \tag{5.3a}$$

$$\cos 2\phi=(b-a)/[(b-a)^2+\Omega^2]^{1/2}. \tag{5.3b}$$

The new Hamiltonian becomes

$$H'=U^{\dagger}HU=\begin{pmatrix}\lambda_- & 0\\ 0 & \lambda_+\end{pmatrix}, \tag{5.4}$$

where

$$\lambda_{\pm}=\tfrac{1}{2}(a+b)\pm\tfrac{1}{2}[(b-a)^2+\Omega^2]^{1/2}. \tag{5.5}$$

The new eigenvalues are located symmetrically about an energy midway between the unperturbed levels a and b. The new levels are further from the midpoint energy than the original levels were, since

$$[(b-a)^2+\Omega^2]^{1/2}\geq|b-a|. \tag{5.6}$$

The laser always tends to move the unperturbed levels further from one another.

This degeneracy-lifting process can now be applied to the two cases in which (2.9) reduces to a quasidegenerate 2×2 matrix weakly coupled to the remainder, namely, $\Omega_1\gg\Omega_2$ and $\Omega_2\gg\Omega_1$.

Let us consider first the case $\Omega_1\gg\Omega_2$, which should be relevant to frame (c) of Figs. 7, 9, and 10. From (2.9) we observe that for $\Omega_1\gg\Omega_2$, Δ levels 1 and 2 are quasidegenerate and weakly coupled to level 3. A unitary transformation of the Schrödinger equation (2.5) of the form

$$U=\begin{pmatrix}\cos\alpha & -\sin\alpha & 0\\ \sin\alpha & \cos\alpha & 0\\ 0 & 0 & 1\end{pmatrix}, \tag{5.7}$$

[where $\sin\alpha$ and $\cos\alpha$ are the same as $\sin\phi$ and $\cos\phi$ above, but with $a=0$, $b=\Delta$, and $\Omega=\Omega_1$], has the effect of diagonalizing (2.9) exactly when $\Omega_2=0$:

$$\overline{W}=U^{\dagger}WU=\begin{pmatrix}\lambda_- & 0 & -\tfrac{1}{2}\Omega_2\sin\alpha\\ 0 & \lambda_+ & -\tfrac{1}{2}\Omega_2\cos\alpha\\ -\tfrac{1}{2}\Omega_2\sin\alpha & -\tfrac{1}{2}\Omega_2\cos\alpha & 2\Delta-i\tfrac{1}{2}R\end{pmatrix}, \tag{5.8}$$

where

$$\lambda_{\pm}=\tfrac{1}{2}\Delta\pm\tfrac{1}{2}(\Delta^2+\Omega_1^2)^{1/2}. \tag{5.9}$$

The new diagonal elements $\lambda_{\pm}$ are the usual "dressed"-atom energy levels. The coupling of these levels to level 3 is through Rabi frequency Ω_2. If $|\Delta|\ll\Omega_1$, then these levels are equally coupled to level 3. If $|\Delta|\gg\Omega_1$, then the original Hamiltonian had no quasidegeneracy. However, having dressed the atomic states, when $|\Delta|\gg\Omega_1$ the coupling of level 3 is stronger to dressed level 1 when Δ is negative, and stronger to dressed level 2 when Δ is positive.

The equations of motion for the amplitudes C_i associated with the energy levels E_i are obtained from the Schrödinger equation in the standard way:

$$\dot{C}_1=i\tfrac{1}{2}\Omega_2\sin\alpha e^{-i(2\Delta-\lambda_-)t}e^{-(R/2)t}C_3, \tag{5.10a}$$

$$\dot{C}_2=i\tfrac{1}{2}\Omega_2\cos\alpha e^{-i(2\Delta-\lambda_+)t}e^{-(R/2)t}C_3, \tag{5.10b}$$

$$\dot{C}_3=i\tfrac{1}{2}\Omega_2(\sin\alpha e^{i(2\Delta-\lambda_-)t}e^{(R/2)t}C_1 +\cos\alpha e^{i(2\Delta-\lambda_+)t}e^{(R/2)t}C_2). \tag{5.10c}$$

where

$$\overline{\psi}(t)=\begin{pmatrix}C_1e^{-i\lambda_-t}\\ C_2e^{-i\lambda_+t}\\ C_3e^{-i(2\Delta)t}e^{-(R/2)t}\end{pmatrix}, \tag{5.11}$$

$$\overline{\psi}(0)=U^{\dagger}\begin{pmatrix}1\\0\\0\end{pmatrix}=\begin{pmatrix}\cos\alpha\\-\sin\alpha\\0\end{pmatrix}. \tag{5.12}$$

If we set $C_1=0$ in (5.10), then (5.10b) and (5.10c) are the equations of motion describing a two-level atom undergoing ionization. The Rabi frequency Ω, detuning δ, and ionization rate γ of that two-level atom are

$$\Omega=\Omega_2\cos\alpha, \tag{5.13a}$$

$$\delta=2\Delta-\lambda_+, \tag{5.13b}$$

$$\gamma=R. \tag{5.13c}$$

If we set $C_2=0$ in (5.10), then (5.10a) and (5.10c) are the equations of motion describing another two-level atom undergoing ionization, with the parameters

$$\Omega=\Omega_2\sin\alpha, \tag{5.14a}$$

$$\delta=2\Delta-\lambda_-, \tag{5.14b}$$

$$\gamma=R. \tag{5.14c}$$

Since the effective population precession frequencies $(\delta^2+\Omega^2)^{1/2}$ for each of these two-level sets of equations are always significantly different, except at resonance, *there is in most cases negligible coherent coupling between the populations gov-*

erned by each of these sets of equations. We now go one step further and assert that the amplitude C_3 may be split into two parts C_{31} and C_{32} that couple only to the amplitudes C_1 and C_2, respectively. Then the three Eqs. (5.10) become two independent sets of two equations

$$\dot{C}_1=\tfrac{1}{2}i\Omega_2\sin\alpha e^{-i(2\Delta-\lambda_-)t}e^{-(R/2)t}C_{31}, \tag{5.15a}$$

$$\dot{C}_{31}=\tfrac{1}{2}i\Omega_2\sin\alpha e^{i(2\Delta-\lambda_-)t}e^{(R/2)t}C_1, \tag{5.15b}$$

$$\dot{C}_2=\tfrac{1}{2}i\Omega_2\cos\alpha e^{-i(2\Delta-\lambda_+)t}e^{-(R/2)t}C_{32}, \tag{5.16a}$$

$$\dot{C}_{32}=\tfrac{1}{2}i\Omega_2\cos\alpha e^{i(2\Delta-\lambda_+)t}e^{(R/2)t}C_2. \tag{5.16b}$$

The initial population in each set is determined by the dressed-atom transformation (5.12).

Now, with respect to these two uncoupled two-level systems, we recall that the solution for the total bound probability of a two-level atom undergoing ionization from the upper level at rate γ (while being pumped from the lower level by a laser detuned by δ and with Rabi frequency Ω) is approximately

$$P(t)=P(0)(\cos^2 z e^{-(\gamma\sin^2 z)t}+\sin^2 z e^{-(\gamma\cos^2 z)t}), \tag{5.17a}$$

where

$$\cos 2z=\delta/(\delta^2+\Omega^2)^{1/2}. \tag{5.17b}$$

The approximation used here relies on the validity of the inequality $\Omega\gg\gamma$, an inequality that is well satisfied in the numerical examples treated below. Therefore the solutions to Eqs. (5.15) and (5.16) are

$$P_{1,3}(t)=\cos^2\alpha(\cos^2 z_1 e^{-(R\sin^2 z_1)t}+\sin^2 z_1 e^{-(R\cos^2 z_1)t}), \tag{5.18}$$

$$P_{2,3}(t)=\sin^2\alpha(\cos^2 z_2 e^{-(R\sin^2 z_2)t}+\sin^2 z_2 e^{-(R\cos^2 z_2)t}), \tag{5.19}$$

where $P_{1,3}(t)=|C_1(t)|^2+|C_{31}(t)|^2$, etc., and

$$\cos 2z_1=\frac{2\Delta-\lambda_-}{[(2\Delta-\lambda_-)^2+(\Omega_2\sin\alpha)^2]^{1/2}}, \tag{5.20a}$$

$$\cos 2z_2=\frac{2\Delta-\lambda_+}{[(2\Delta-\lambda_+)^2+(\Omega_2\cos\alpha)^2]^{1/2}}. \tag{5.20b}$$

The ionization probability is

$$P_{\text{ion}}=1-P_{1,3}(t)-P_{2,3}(t). \tag{5.21}$$

In all cases the solutions (5.18) and (5.19) can be approximated by a single exponential:

$$P_{1,3}(t)\sim\cos^2\alpha\exp[-\tfrac{1}{2}R(1-|\cos 2z_1|)t], \tag{5.22}$$

$$P_{2,3}(t)\sim\sin^2\alpha\exp[-\tfrac{1}{2}R(1-|\cos 2z_2|)t]. \tag{5.23}$$

An important feature of the numerical solutions is contained in Eqs. (5.20). Note that each expression involves a resonant denominator. As a consequence, resonances in the ionization rate appear at $2\Delta=\lambda_\pm$, that is, for the detuning values

$$\Delta_R=\pm\Omega_1/2\sqrt{2}\,. \tag{5.24}$$

These resonances, appearing symmetrically about $\Delta=0$, arise from the ac Stark effect. Upon substituting the parameters of Fig. 10(c) into (5.22)–(5.24), we find

$$\Delta_R=\pm 0.707, \tag{5.25a}$$

$$P_{\text{ion}}(\Delta=0, Rt=10)=0.27, \tag{5.25b}$$

$$P_{\text{ion}}(\Delta=\Delta_R, Rt=10)=0.35. \tag{5.25c}$$

After normalization to the heights of the Doppler profile at $\Delta=0$ and $\Delta=\Delta_R$ these values are in good agreement with Fig. 10(c).

The time dependence of the bound probability for the two channels (5.22) and (5.23) is described in each case by a single rate. At either resonance one channel is described by a rate corresponding to the strong-field limit and the other by a rate corresponding to the weak-field limit. In all other regions, away from the two resonances, both are described by a weak-field limit rate. Interference between these channels, as we asserted in deriving (5.15) and (5.16) is small. The transition region between resonance and far off resonance is the region where the error in (5.22) or (5.23) is greatest.

The population in each channel (5.22) and (5.23) is determined by the "dressed" atom transformation (5.12). As the population increases in either channel with changing detuning, the rate of ionization decreases. On a resonance the population ionized readily at rate $\frac{1}{2}R$ is always $\frac{1}{3}$. For very large Ω_1 the detuning scan without the Doppler-profile weight factor would appear as two peaks. For any fixed large time, as Ω_1 increases, the width of the peak increases proportional to Ω_1. As the peaks move into the tails of the Doppler profile the overall ionization decreases.

It is interesting to observe how much closer to the underlying physics one gets by making the "dressing" transformation (5.7). In Fig. 11 we show the results of two numerical calculations of the same ionization probabilities, one calculation proceeding from the original Hamiltonian (2.9) and the other from the "dressed" Hamiltonian (5.8). The smoothness of the curves in Fig. 11(b) is graphic justification for the use in dressed-atom calculations[6] of perturbation theory based on dressed zero-order eigenstates.

Next we consider the case $\Omega_2\gg\Omega_1$. It is apparent from a comparison of Figs. 7(c) and 7(e) that different results are to be expected. However, the basic principle of our analytic method remains valid. Because Ω_2 is so large, there is an effec-

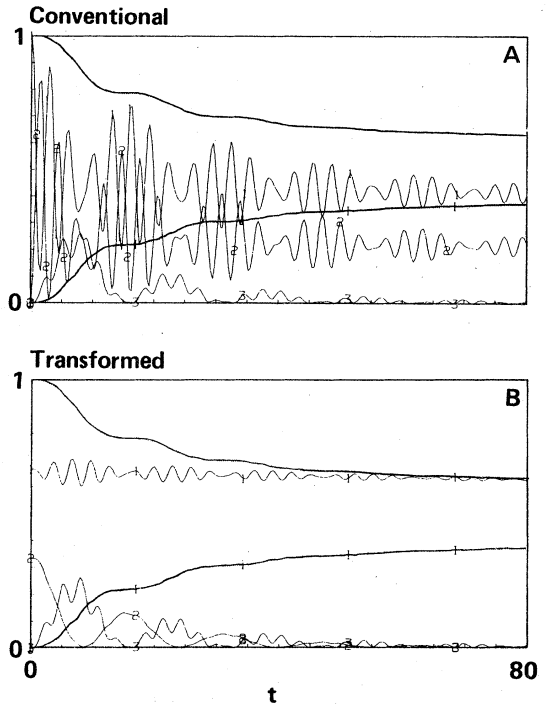

FIG. 11. Comparison of the three-level population time dependences before and after the dresssing transformation (5.7).

tive degeneracy of levels 2 and 3 [cf. W in Eq. (2.9)]. We begin by removing this quasidegeneracy by applying the transformation

$$U=\begin{pmatrix}1 & 0 & 0\\ 0 & \cos\chi & -\sin\chi\\ 0 & \sin\chi & \cos\chi\end{pmatrix}, \tag{5.26a}$$

$$U^{-1}=\begin{pmatrix}1 & 0 & 0\\ 0 & \cos\chi & \sin\chi\\ 0 & -\sin\chi & \cos\chi\end{pmatrix}, \tag{5.26b}$$

where $\sin\chi$ and $\cos\chi$ are the same as $\sin\phi$ and $\cos\phi$ in (5.3), with the replacements $b\to a\to(\Delta-\frac{1}{2}iR)$ and $\Omega\to\Omega_2$. This transformation would diagonalize W in (2.9) exactly if Ω_1 were zero:

$$\overline{W}=U^{-1}WU=\begin{pmatrix}0 & -\frac{1}{2}\Omega_1\cos\chi & \frac{1}{2}\Omega_1\sin\chi\\ -\frac{1}{2}\Omega_1\cos\chi & \Delta+\kappa_- & 0\\ \frac{1}{2}\Omega_1\sin\chi & 0 & \Delta+\kappa_+\end{pmatrix}. \tag{5.27}$$

Here the presence of R leads to complex eigenvalues

$$\kappa_\pm=\tfrac{1}{2}(\Delta-\tfrac{1}{2}iR)\pm\tfrac{1}{2}[\Omega_2^2+(\Delta-\tfrac{1}{2}iR)^2]^{1/2}. \tag{5.28}$$

Also, the transformation of the Schrödinger equation is not unitary since $U^{-1}\neq U^\dagger$.

The equations of motion for the amplitudes C_i are obtained from the Schrödinger equation in the standard way:

$$\dot{C}_1=\tfrac{1}{2}i\Omega_1(\cos\chi e^{-i(2\Delta-\mu_+)t}C_2-\sin\chi e^{-i(2\Delta-\mu_-)t}C_3, \tag{5.29a}$$

$$\dot{C}_2=\tfrac{1}{2}i\Omega_1\cos\chi e^{i(2\Delta-\mu_+)t}C_1, \tag{5.29b}$$

$$\dot{C}_3=-\tfrac{1}{2}i\Omega_1\sin\chi e^{i(2\Delta-\mu_-)t}C_1, \tag{5.29c}$$

where

$$\Delta-\mu_\pm=\kappa_\mp, \tag{5.30}$$

$$\overline{\psi}(t)=\begin{pmatrix}C_1\\ C_2e^{-i(2\Delta-\mu_+)t}\\ C_3e^{-i(2\Delta-\mu_-)t}\end{pmatrix}, \tag{5.31}$$

$$\overline{\psi}(0)=U^{-1}\begin{pmatrix}1\\0\\0\end{pmatrix}=\begin{pmatrix}1\\0\\0\end{pmatrix}. \tag{5.32}$$

For small R we find

$$\cos\chi\sim\frac{1}{\sqrt{2}}\left(1+\frac{\Delta}{(\Delta^2+\Omega_2^2)^{1/2}}\right)^{1/2}, \tag{5.33a}$$

$$\sin\chi\sim\frac{1}{\sqrt{2}}\left(1-\frac{\Delta}{(\Delta^2+\Omega_2^2)^{1/2}}\right)^{1/2}, \tag{5.33b}$$

$$\mu_\pm\sim\lambda_\pm+\tfrac{1}{2}iR\begin{pmatrix}\sin^2\chi\\ \cos^2\chi\end{pmatrix}, \tag{5.34}$$

$$\lambda_\pm\equiv\tfrac{1}{2}\Delta\pm\tfrac{1}{2}(\Delta^2+\Omega_2^2)^{1/2}. \tag{5.35}$$

Here $\sin\chi$ and $\cos\chi$ are the usual dressed-atom transformation functions, and the eigenvalues $\mu_\pm$ are the usual dressed-atom eigenvalues $\lambda_\pm$ plus a small additional positive imaginary part.

If we set $C_2=0$ in (5.29), then (5.29a) and (5.29c) are the equations of motion describing a two-level atom undergoing ionization. The Rabi frequency Ω, detuning δ, and ionization rate γ are

$$\Omega=-\Omega_1\sin\chi, \tag{5.36a}$$

$$\delta=2\Delta-\lambda_-, \tag{5.36b}$$

$$\gamma=R\cos^2\chi. \tag{5.36c}$$

If $C_2=0$ in (5.29), then (5.29a) and (5.29b) are the equations of motion describing a two-level atom undergoing ionization with the parameters

$$\Omega=\Omega_1\cos\chi, \tag{5.37a}$$

$$\delta=2\Delta-\lambda_+, \tag{5.37b}$$

$$\gamma=R\sin^2\chi. \tag{5.37c}$$

Just as in the case $\Omega_1 \gg \Omega_2$ we assert that coherent coupling between the populations governed by each of these sets of equations is always negligible.

By splitting the amplitude C_1 into two parts, C_{12} and C_{13}, the two independent sets of equations become

$$\dot{C}_{12}=\tfrac{1}{2}i\Omega_1\cos\chi e^{-i(2\Delta-\lambda_+)t}e^{-(R/2)\sin^2\chi t}C_2, \tag{5.38a}$$

$$\dot{C}_2=\tfrac{1}{2}i\Omega_1\cos\chi e^{i(2\Delta-\lambda_+)t}e^{+(R/2)\sin^2\chi t}C_{12}, \tag{5.38b}$$

$$\dot{C}_{13}=-\tfrac{1}{2}i\Omega_1\sin\chi e^{-i(2\Delta-\lambda_-)t}e^{-(R/2)\cos^2\chi t}C_3, \tag{5.39a}$$

$$\dot{C}_3=-\tfrac{1}{2}i\Omega_1\sin\chi e^{i(2\Delta-\lambda_-)t}e^{+(R/2)\cos^2\chi t}C_{13}. \tag{5.39b}$$

The general solution to (5.38) and (5.39) is given in (5.17). These solutions are

$$P_1(t)=P_1(0)(\cos^2 z_1 e^{-\sin^2\chi(R\sin^2 z_1)t} + \sin^2 z_1 e^{-\sin^2\chi(R\cos^2 z_1)t}), \tag{5.40}$$

$$P_2(t)=P_2(0)(\cos^2 z_2 e^{-\cos^2\chi(R\sin^2 z_2)t} + \sin^2 z_2 e^{-\cos^2\chi(R\cos^2 z_2)t}), \tag{5.41}$$

where

$$\cos 2z_1=\frac{2\Delta-\lambda_+}{[(2\Delta-\lambda_+)^2+(\Omega_1\cos\chi)^2]^{1/2}}, \tag{5.42a}$$

$$\cos 2z_2=\frac{2\Delta-\lambda_-}{[(2\Delta-\lambda_-)^2+(\Omega_1\sin\chi)^2]^{1/2}}. \tag{5.42b}$$

In all cases the solutions (5.40) and (5.41) can be approximated by a single exponential:

$$P_1(t)\sim P_1(0)\exp[-\tfrac{1}{2}R\sin^2\chi(1-|\cos 2z_1|)t], \tag{5.43}$$

$$P_2(t)\sim P_2(0)\exp[-\tfrac{1}{2}R\cos^2\chi(1-|\cos 2z_2|)t]. \tag{5.44}$$

Since both channels are described by a single rate and share the population in the ground state 1, we require the total bound probability to be of the form of a single exponential whose rate is the sum of the rates given in (5.43) and (5.44)

$$P_{\text{bound}}(t)\simeq\exp[-\tfrac{1}{2}Rt(1-\cos^2\chi|\cos 2z_2|-\sin^2\chi|\cos 2z_1|)]. \tag{5.45}$$

From (5.42) we see that the resonances occur at

$$2\Delta-\lambda_\pm=0, \tag{5.46}$$

and this reduces, as before, to

$$\Delta_R=\pm\Omega_2/2\sqrt{2}. \tag{5.47}$$

Substituting the parameters of Fig. 10(e) into (5.33), (5.35), (5.42), (5.45), and (5.47) we find the resonant frequencies to have the values

$$\Delta_R=\pm 0.707 \tag{5.48a}$$

and the corresponding value of the ionization to be

$$P_{\text{ion}}(\Delta_R, Rt=10)=0.82 \tag{5.48b}$$

These are both in good agreement with Fig. 10(e) after normalizing to the height of the Doppler curve at the Stark peak.

Comparing (5.48a) and (5.25a), we see the location of the resonances is independent of which laser is more intense. This symmetric structure was illustrated in Figs. 10(c) and 10(e). The difference in the amplitudes of the resonances in Figs. 10(c) and 10(e) is easily understood after comparing (5.45) with (5.22) and (5.23). For $\Omega_1 \gg \Omega_2$ the two independent channels leading to ionization share the population in level 1: one channel has $\cos^2\psi$ population and the other has $\sin^2\psi$ population. The dressed-atom transformation which couples levels 1 and 2 determines the strength of the two channels. For $\Omega_2 \gg \Omega_1$, there are also two independent channels leading to ionization, but all the population is available to each channel. The rate out of the initially totally populated level 1 is simply the sum of the two rates governing each channel. The ionization is therefore greater for $\Omega_2 \gg \Omega_1$.

VI. COUNTERPROPAGATING BEAMS

The preceding examples dealt with excitation steps whose frequency shifts accumulated: a shift of Δ in each step gave a cumulative detuning 2Δ after two steps. We now consider the case when the second shift opposes the first shift, so that the two produce a null cumulative detuning. Such cancellation occurs with counterpropagating laser beams, if the detunings originate from the Doppler distribution of velocities. That is, if $\hat{n}\omega_1/c$ and $-\hat{n}\omega_2/c$ are the wave vectors of the two laser beams, then for an atom with velocity v along $\hat{n}$ we have $\Delta_1=\omega_1 v/c$ and $\Delta_2=-\omega_2 v/c$. As before, we assume that the difference $\Delta_1-\Delta_2$ is much smaller than any other frequency and neglect it. We put $\Delta_1+\Delta_2\approx 0$. This case has been studied both analytically and numerically by Hodgkinson and Briggs[11] in the population conserving ($R=0$) limit.

A. Numerical experiments

The exactly resonant members of the statistical ensemble cannot distinguish between copropagating and counter-propagating lasers; Fig. 7 applies in both cases. However, the Doppler averages $\bar{P}_n(t)$ shown in Fig. 12 for counterpropagating lasers differ appreciably from the curves of Fig. 9 for copropagating lasers. This difference is most pronounced in Figs. 12(a) and 9(a), where both transitions have equal Rabi frequency. In Figs. 12(a) and 9(a) we see that Doppler averaging damps out the population oscillations, just as in the copropagating case, but that the ionization proceeds almost as effectively as in the resonant case, shown in Fig. 7(a). This is because, for any detuning, the condition $\Delta_1+\Delta_2\approx 0$ maintains

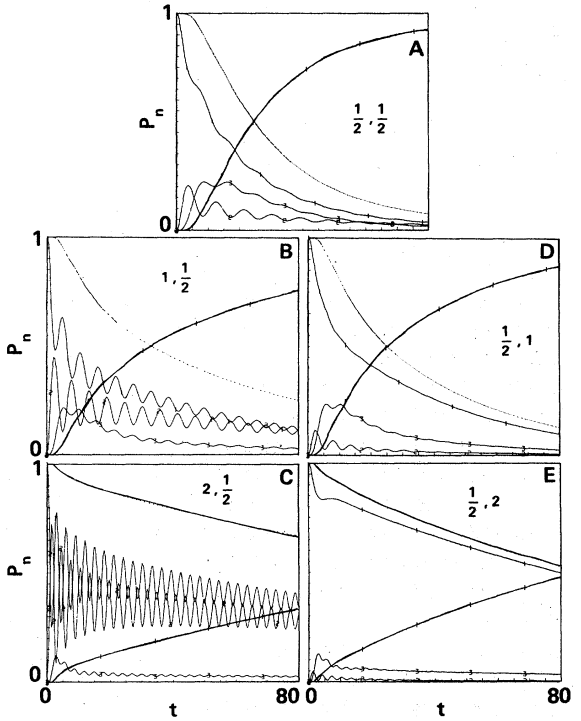

FIG. 12. Population averages $\bar{P}_n(t)$ over Doppler distribution for counter-propagating lasers, $T^*=1$. Parameters as in Fig. 6.

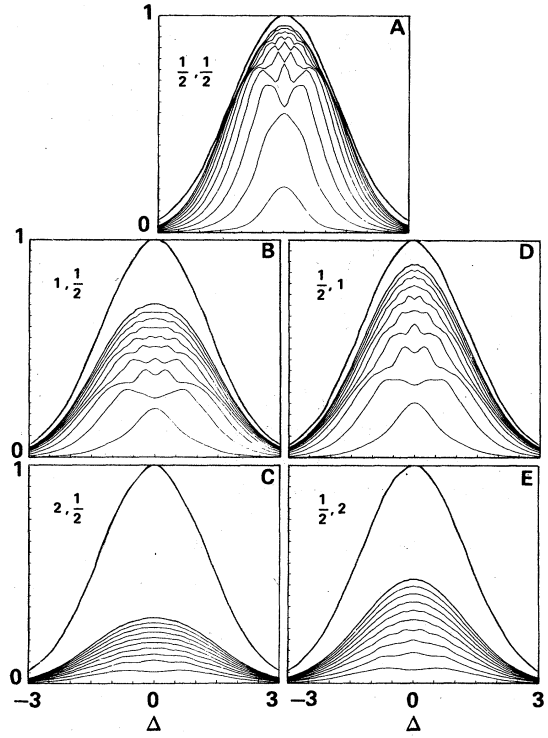

FIG. 13. Relative ionization probability $P_{\text{ion}}(t;\Delta)$ at successive times, as a function of detuning, for counter-propagating beams. Parameters as in Fig. 6.

an exact two-photon resonance between the ground state and the ionizing level 3.

As either Rabi frequency is increased the averaged ionization curves $\bar{P}_{\text{ion}}(t)$ for counterpropagating and copropagating lasers begin to look alike. This is because all of the atoms behave more and more like on-resonant atoms as the Rabi frequencies (and thus the power broadenings) are increased. However, the details of individual population averages differ appreciably. This difference is most striking when the second Rabi frequency is the larger; Doppler averaging then damps out almost all the oscillation in level 1.

The differences between copropagating and counterpropagating lasers is particularly striking in plots of ionization versus detuning, as in Fig. 13. The ripples here are caused by Rabi oscillations; the ac Stark-effect splitting of the copropagating case, shown in Figs. 10(c) and 10(e), is not evident. We also see that the total ionization is less dependent upon which laser is the stronger—in contrast to the copropagating case where ionization is favored by a strong second laser.

B. Theoretical analysis

Just as in the copropagating case, some features of the population dynamics can be subjected to a dressed-atom analysis. Such an analysis can be carried through in a relatively simple way whenever one of the Rabi frequencies dominates the other. In the following several paragraphs we analyze the counterpropagating dynamics with a view to explaining features of Figs. 13(c) and 13(e), in particular the level of ionization on resonance and the absence of the Stark splitting seen in Figs. 10(c) and 10(e). Our analysis generalizes that of Hodgkinson and Briggs[11] to the case where losses are present ($R\neq 0$).

For counterpropagating lasers, $\Delta_1+\Delta_2=0$. This creates a degeneracy between the energies of levels 1 and 3 if the weak ionization rate R is neglected in (2.9). We therefore look for a solution of the Schrödinger equation after applying the following unitary transformation, which removes the degeneracy:

$$U=\begin{pmatrix}\cos\psi & 0 & -\sin\psi\\ 0 & 1 & 0\\ \sin\psi & 0 & \cos\psi\end{pmatrix}, \tag{6.1}$$

where

$$\cos\psi=\Omega_2/(\Omega_1^2+\Omega_2^2)^{1/2}, \tag{6.2a}$$

$$\sin\psi=-\Omega_1/(\Omega_1^2+\Omega_2^2)^{1/2}. \tag{6.2b}$$

The new Hamiltonian $\bar{W}=U^{-1}WU$ becomes

$$\overline{W}=\begin{pmatrix} -\frac{1}{2}iR\sin^2\psi & 0 & -\frac{1}{2}iR\sin\psi\cos\psi \\ 0 & \Delta & \frac{1}{2}\Omega_1\sin\psi-\frac{1}{2}\Omega_2\cos\psi \\ -\frac{1}{2}iR\sin\psi\cos\psi & \frac{1}{2}\Omega_1\sin\psi-\frac{1}{2}\Omega_2\cos\psi & -\frac{1}{2}iR\cos^2\psi \end{pmatrix} \tag{6.3}$$

and

$$\overline{\psi}(0)=\begin{pmatrix} \cos\psi \\ 0 \\ -\sin\psi \end{pmatrix}. \tag{6.4}$$

If $\Omega_1 \gg \Omega_2$, then $|\sin\psi| \gg |\cos\psi|$, and vice versa. In either case the product $\sin\psi\cos\psi$, is small and the off-diagonal coupling between levels 1 and 3 can be neglected completely:

$$\overline{W}\cong\begin{pmatrix} -\frac{1}{2}iR\sin^2\psi & 0 & 0 \\ 0 & \Delta & -\frac{1}{2}\Omega \\ 0 & -\frac{1}{2}\Omega & -\frac{1}{2}iR\cos^2\psi \end{pmatrix} \tag{6.5}$$

where

$$\Omega=(\Omega_1^2+\Omega_2^2)^{1/2}. \tag{6.6}$$

The unitary transformation and the approximations made in obtaining (6.5) imply that the dynamics are dominated by the double quantum transition 1–3. Since one of the lasers is being assumed weak, the two-step transition coupling does not appear in (6.5). The population has two channels for ionization. Channel 1, which dominates if $\Omega_1 \gg \Omega_2$, depends on the detuning Δ of laser 1. Channel 2, which dominates if $\Omega_2 \gg \Omega_1$, is independent of level 2. Far off resonance the coupling to level 2 is negligible, making channels 1 and 2 equivalent.

The Schrödinger equation, which is governed by the Hamiltonian (6.5) for the state vector

$$\overline{\psi}(t)=\begin{pmatrix} C_1(t) \\ C_2(t) \\ C_3(t) \end{pmatrix}, \tag{6.7}$$

is easily solved, but the solutions are very complicated. Therefore, we will exhibit only the solutions on resonance and far off resonance. On resonance, when $\Delta=0$, we find

$$|C_1|^2\cong\cos^2\psi\exp(-R\sin^2\psi)t, \tag{6.8a}$$

$$|C_2|^2\cong\sin^2\psi\exp(-\tfrac{1}{2}R\cos^2\psi)t\sin^2\tfrac{1}{2}\Omega t, \tag{6.8b}$$

$$|C_3|^2\cong\sin^2\psi\exp(-\tfrac{1}{2}R\cos^2\psi)t\cos^2\tfrac{1}{2}\Omega t. \tag{6.8c}$$

Far off resonance the approximate solutions are

$$|C_1|^2\simeq\cos^2\psi e^{-(R\sin^2\psi)t}, \tag{6.9a}$$

$$|C_2|^2\cong 0, \tag{6.9b}$$

$$|C_3|^2\cong\sin^2\psi e^{-(R\cos^2\psi)t}. \tag{6.9c}$$

On resonance the population in levels 2 and 3 is very rapidly oscillating between these levels, effectively reducing the ionization rate by a factor of $\frac{1}{2}$ in (6.8b) and (6.8c). Far off resonance very little population reaches level 2, making the 2-3 ionization rate formally equivalent to the 1 ionization rate; compare (6.9a) and (6.9b). These results, with $R=0$, give the time-dependences underlying the time-averaged results obtained recently by Hodgkinson and Briggs.[11] Our Doppler-averaged curves in Figs. 12 and 13 show the influence that a finite population loss rate R has on the loss-free time-averaged populations of Ref. 11.

Upon substituting the parameters of Fig. 12(c) into (6.8), we find the ionization probability on resonance to be

$$P_I(Rt=10)=1-\sum_{i=1}^{3}|C_i|^2=0.28 \tag{6.10}$$

which is in excellent agreement with Fig. 12(c). Far off resonance the ionization probability is independent of which is greater, Ω_1 or Ω_2; compare the tails of the ionization curves in Figs. 13(c) and 13(e). Upon substituting the parameters of Fig. 13(e) into (6.8) or (6.9) we find the ionization probability (which is independent of Δ):

$$P_I(Rt=10)=0.46 \tag{6.11}$$

which is in excellent agreement with Fig. 13(e) for each detuning, after taking into account the Doppler profile. The independence of the ionization as a function of detuning is due entirely to the fact that $\Omega_2 \gg \Omega_1$.

The difference in the on-resonance ionization for $\Omega_1 \gg \Omega_2$ and $\Omega_2 \gg \Omega_1$ is now easily understood from (6.8). For $\Omega_1 \gg \Omega_2$ the ionization occurs at a rate which is $\frac{1}{2}$ the rate of ionization when $\Omega_2 \gg \Omega_1$. The difference is due to the coupling to level 2 which exists when $\Omega_1 \gg \Omega_2$. In this case the population of level 1 is almost zero. The majority of the population is shared equally between levels 2 and 3. Thus, ionization occurs only from level 3, reducing the ionization rate by a factor of 2.

VII. SUMMARY

We have presented numerical solutions as well as nonperturbative analytic expressions for the

population lost from a two-laser-excited statistically broadened three-level quantum system. These expressions are valid for large or small detuning of the two lasers, in the limit that laser-stimulated processes dominate spontaneous ones. The numerical results reflect the strong smoothing influence on the overall population dynamics of the statistical distribution of transition frequencies. Nevertheless, the coherent effect of dynamic Stark splitting is clearly evident even after the statistical averages are computed.

A general rule found for relative laser powers, to produce most efficient population loss, $\Omega_2>\Omega_1$, is reminiscent of earlier findings[4,5] based on investigations of homogeneously (nonstatistically) broadened three-level systems. The analytic results of Sec. V can be regarded as generalizations of some of the two-laser on-resonance findings of Cohen-Tannoudji and Reynaud.[6] The complexity of their three dressed states is avoided by our off-resonance assumption, first encountered in going from Eqs. (5.10) to Eqs. (5.15) and (5.16). The utility of this assumption, even at resonance, is illustrated by the agreement, usually within several percent, between the approximate analytic and exact numerical results.

A superficial contrast to the general rule $\Omega_2>\Omega_1$ is provided by the case of counterpropagating lasers. Hodgkinson and Briggs have shown[11] analytically in both limits $T^*\to 0$ and $T^*\to\infty$ that in the absence of population loss ($R=0$) the population of level 3 is maximized when $\Omega_2=\Omega_1$.

However, the existence of reactivity itself modifies this conclusion, and it can be considered reliable only at low laser powers [as in Fig. 13(a)], The reason for this can be seen in Eqs. (6.8) and (6.9). At low powers, almost all atoms are far off resonance and Eqs. (6.9) show that the population remaining in the atom is minimized (reactivity is maximized) when $\cos^2\psi=\sin^2\psi$, i.e., when $\Omega_2=\Omega_1$. On the other hand, in the more interesting high-power case, a significant fraction of the atoms are power broadened into near resonance, and Eqs. (6.8) apply. In that case, for Rt not too small, maximum reactivity is achieved for $\Omega_2^2=2\Omega_1^2$. Thus, we find again, even in the Doppler-free case, that the second laser should be the more powerful for the greatest degree of population loss (ionization, dissociation, chemical reaction, etc.) from the three-level system.

ACKNOWLEDGMENT

This work was performed under the auspices of the U.S. Department of Energy under contract No. W-7405-Eng-48.

---

*Visiting Fellow 1977–1978. Permanent address: Dept. of Physics and Astronomy, University of Rochester, Rochester, N. Y. 14627.

[1]See, for example, L. Allen and J. H. Eberly, *Optical Resonance and Two-Level Atoms* (Wiley, New York, 1975), Chaps. 2 and 3.

[2]Graphs of time-dependent population flow in a variety of different N-level systems are given in J. H. Eberly, B. W. Shore, Z. Bialynicka-Birula, and I. Bialynicki-Birula, Phys. Rev. A 16, 2038 (1977).

[3]Recently analytic studies of N-level systems, for arbitrary N, have become available. See, for example, V. S. Letokhov and A. A. Makarov, Opt. Commun. 17, 250 (1976); D. M. Larsen and N. Bloembergen, *ibid.* 17, 254 (1976); Z. Bialynicka-Birula, I. Bialynicki-Birula, J. H. Eberly, and B. W. Shore, Phys. Rev. A 16, 2048 (1977); B. W. Shore and J. H. Eberly, Opt. Commun. 24, 83 (1978), P. W. Milonni and J. H. Eberly, J. Chem. Phys. 68, 1602 (1968); V. S. Letokhov and A. A. Makarov, Appl. Phys. 16, 47 (1978).

[5]This is illustrated, for example, by B. W. Shore and J. R. Ackerhalt, Phys. Rev. A 15, 1640 (1977). See expecially Fig. 2.

[6]See Ref. 5; and J. R. Ackerhalt and B. W. Shore, Phys. Rev. A 16, 277 (1977). The dressed-atom approach to a variety of three-level problems is explored by R. M. Whitley and C. R. Stroud, Jr. [Phys. Rev. A 14, 1498 (1976)]; C. Cohen-Tannoudji and S. Reynaud [J. Phys. B 10, 2311 (1977)]; and R. Kornblith and J. H. Eberly [J. Phys. B 11, 1545 (1978).

[7]These complications are mentioned, but not treated, by S. Feneuille and M.-G. Schweighofer in J. Phys. 36, 781 (1975). In their terms, we are studying the case where strong optical pumping effects and velocity effects are simultaneously important. In addition, we have a type of optical pumping not contemplated by Feneuille and Schweighofer, or by other earlier workers who discussed spectroscopic effects in three-level systems [see, for example, A. Schabert, R. Keil, and P. E. Toschek, Appl. Phys. 6, 181 (1975), and references given there]. In our case, the reaction-collection step can be thought of as optical pumping to a trapping state, a state that does not return its population to the ground level or any other level of the system.

[8]If the laser intensities are great enough, we should expect the level-to-level absorption rates to dominate the irreversible reaction-collection rate at the last level. In this limit our three-level model is relevant to optical Autler-Townes spectroscopic experiments in which a reaction-collection step is absent: A. Schabert *et al.*, Ref. 7; A. Schabert, R. Keil, and P. E. Toschek, Opt. Commun. 13, 265 (1975); Ph. Cahuzac and R. Vetter, Phys. Rev. A 14, 170 (1976); and J. L. Piqué and J. Pinard, J. Phys. B 9, L77 (1976). An experiment that clearly revealed Autler-Townes effects, i.e., dynamic Stark splitting, in a three-level system

that included a reaction-collection step (ionization) but not Doppler broadening has been reported by S. E. Moody and M. Lambropoulos [Phys. Rev. A 15, 1497 (1977)].

[9]The dynamic Stark effect was observed in microwave absorption and analyzed by S. H. Autler and C. H. Townes [Phys. Rev. 100, 703 (1955)]. The comparable optical effect has been analyzed by Feneuille and Schweighofer (Ref. 7), and a number of optical-absorption observations have been reported (Ref. 8). The observation of the dynamic Stark effect in emission is not feasible at microwave frequencies, and was first accomplished recently using optical transitions in sodium atoms in an atomic beam: F. Schuda, C. R. Stroud, Jr., and M. Hercher, J. Phys. B 7, L198 (1974).

[10]Autler and Townes, Ref. 9; E. T. Jaynes and F. W. Cummings, Proc. IEEE 51, 89 (1963); C. Cohen-Tannoudji and S. Haroche, J. Phys. 30, 153 (1969). See also papers by Whitley and Stroud, Cohen-Tannoudji and Reynaud, and Kornblith and Eberly, Ref. 6.

[11]D. P. Hodgkinson and J. S. Briggs, Opt. Commun. 22, 45 (1977). See Eq. (8) in particular; but some care is needed in comparing it with our Eqs. (6.8) and (6.9) because our equations refer to the three-level populations after the dressing transformation (6.1).